ORIGINAL ARTICLE

In vivo imaging of the 18-kDa translocator protein (TSPO) with [^{18}F]FEDAA1106 and PET does not show increased binding in Alzheimer's disease patients

Andrea Varrone · Patrik Mattsson · Anton Forsberg · Akihiro Takano ·
Sangram Nag · Balázs Gulyás · Jacqueline Borg · Ronald Boellaard ·
Nabil Al-Tawil · Maria Eriksdotter · Torsten Zimmermann · Marcus Schultze-Mosgau ·
Andrea Thiele · Anja Hoffmann · Adriaan A. Lammertsma · Christer Halldin

Abstract

Purpose Imaging the 18-kDa translocator protein (TSPO) is considered a potential tool for in vivo evaluation of microglial activation and neuroinflammation in the early stages of Alzheimer's disease (AD). ((R)-1-(2-chlorophenyl)-N-[^{11}C]-methyl-N-(1-methylpropyl)-3-iso-quinoline caboxamide ([^{11}C]-(R)-PK11195) has been widely used for PET imaging of TSPO and, despite its low specific-to-nondisplaceable binding ratio, increased TSPO binding has been shown in AD patients. The high-affinity radioligand N-(5-fluoro-2-phenoxyphenyl)-N-(2-[^{18}F]fluoroethyl-5-methoxybenzyl)acetamide ([^{18}F] FEDAA1106) has been developed as a potential in vivo imaging tool for better quantification of TSPO binding. The aim of this study was to quantify in vivo binding of [^{18}F]FEDAA1106 to TSPO in control subjects and AD patients.

Methods Seven controls (five men, two women, age 68±3 years, MMSE score 29±1) and nine AD patients (six men, three women, age 69±4 years, MMSE score 25±3) were studied with [^{18}F]FEDAA1106. PET measurements were performed on an ECAT EXACT HR system (Siemens Medical Solutions) in two 60-min dynamic PET sessions with a 30-min interval between sessions. Arterial blood radioactivity was measured using an automated blood sampling system for the first 5 min and using manually drawn samples thereafter. Quantification was performed using both kinetic analysis based on a two-tissue compartment model and Logan graphical analysis. Outcome measures were total distribution volume (V_T) and binding potential ($BP_{ND}=k_3/k_4$). An estimate of nondisplaceable distribution volume was obtained with the Logan graphical analysis using the first 15 min of PET measurements ($V_{ND\ 1\text{-}15\ min}$). Binding potential (BP_{ND}) was also calculated as: $V_T/V_{ND\ 1\text{-}15\ min} - 1$.

Results No statistically significant differences in V_T, k_3/k_4 or BP_{ND} were observed between controls and AD patients.

Conclusion This study suggests that TSPO imaging with [^{18}F]FEDAA1106 does not enable the detection of microglial activation in AD.

A. Varrone (✉) · P. Mattsson · A. Forsberg · A. Takano · S. Nag ·
B. Gulyás · J. Borg · C. Halldin
Karolinska Institutet, Department of Clinical Neuroscience, Centre for Psychiatry Research, Karolinska Hospital, R5:02,
SE-17176 Stockholm, Sweden
e-mail: andrea.varrone@ki.se

R. Boellaard · A. A. Lammertsma
Department of Radiology & Nuclear Medicine,
VU University Medical Center, Amsterdam, The Netherlands

N. Al-Tawil
Karolinska Trial Alliance Phase-I Unit, Karolinska University Hospital, Stockholm, Sweden

M. Eriksdotter
Karolinska Institutet, Department of Neurobiology,
Care Sciences and Society, Division of Clinical Geriatrics, Novum, Stockholm, Sweden

T. Zimmermann · M. Schultze-Mosgau · A. Thiele · A. Hoffmann
Bayer HealthCare AG, Berlin, Germany

🖄 Springer

Introduction

The 18-kDa translocator protein (TSPO) is a multimeric protein located on the outer mitochondrial membrane [1, 2] of several cell types, including macrophages [3], microglia cells [4] and reactive astrocytes [5]. TSPO is implicated in several physiological processes including cholesterol transport and steroidogenesis, mitochondrial respiration, apoptosis and cell proliferation [1]. In the brain, TSPO is considered to be a marker of activated microglia and neuroinflammation [6]. Increased TSPO binding of ((R)-1-(2-chlorophenyl)-N-[11C]-methyl-N-(1-methylpropyl)-3-isoquinoline caboxamide ([11C]-(R)-PK11195), the most widely used radioligand for TSPO imaging, has been demonstrated in several brain disorders, including stroke [7], traumatic brain injury [8], multiple sclerosis [9], Alzheimer's disease (AD) [10] and Parkinson's disease [11]. In the brain of AD patients, microglial activation has been shown to be associated with the presence of amyloid plaques [12]. Activated glial cells are a source of proinflammatory mediators and thus can be a potential target for antiinflammatory therapy in AD [13]. In that context, TSPO imaging can be viewed as a potential tool for the in vivo evaluation of microglial activation and neuroinflammation in the early stages of AD, and also as a target for the evaluation of novel antiinflammatory drugs.

For many years, [11C]-(R)-PK11195 has been the only well-established radioligand for TSPO imaging. However, due to its relatively low affinity ($K_i = 0.77$ nM) [14] and high nonspecific binding, [11C]-(R)-PK11195 does not display optimal properties as a radioligand for TSPO imaging. In the last decade there have been many attempts to develop novel radioligands for TSPO with better imaging properties than those of [11C]-(R)-PK11195 [15].

Amongst these, N-(2,5-[11C]-dimethoxybenzyl)-N-(5-fluoro-2-phenoxyphenyl)acetamide ([11C]DAA1106) [16] and N-(5-fluoro-2-phenoxyphenyl)-N-(2-[18F]fluoroethyl-5-methoxybenzyl)acetamide ([18F]FEDAA1106) [17] are high-affinity radioligands, which were developed as potential in vivo imaging tools for better quantification of TSPO binding. The in vitro affinity of DAA1106 ($K_i = 0.043$ nM) [14] is at least tenfold higher than that of PK11195 and the quantification of [11C]DAA1106 binding to TSPO has been validated in human subjects [18]. In addition, recently increased TSPO binding has been reported in AD patients compared with control subjects using [11C]DAA1106 [19].

FEDAA1106 displays at least twofold higher affinity for TSPO than DAA1106 [17]. Preclinical studies in nonhuman primates have shown higher brain uptake of [18F]FEDAA1106 than of both [11C]-(R)-PK11195 and [11C]DAA1106 [20]. In previous studies, [18F]FEDAA1106 binding to TSPO has been quantified in control subjects [21], together with its human biodistribution and radiation

dosimetry [22]. [18F]FEDAA1106 is a radioligand displaying in human subjects high uptake and slow elimination from the brain. The dosimetry of [18F]FEDAA1106 is similar to that of other [18F]-labelled radioligands. Because of the lack of a reference region, however, the specific signal needs to be quantified using either compartmental analysis with nonlinear square fitting (NLS) or graphical analysis (GA), in both cases including measurement of the arterial plasma input function.

The aim of this study was to quantify in vivo binding of [18F]FEDAA1106 to TSPO in both control subjects and AD patients in order to assess whether increased binding in AD could be detected.

Materials and methods

Subjects

Seven control subjects (five men, two women) and nine AD patients (six men, three women) were included in this study (for details, see Table 1). The study was approved by the Ethics Committee of the Stockholm region and by the Radiation Safety Committee of the Karolinska University Hospital. All subjects gave written informed consent for participation in the study. AD patients were recruited from different memory clinics of the Stockholm region including the memory clinic at the Karolinska University Hospital, Huddinge. Control subjects were recruited by local advertisement and from a database at the Karolinska Trial Alliance in Stockholm. All subjects underwent careful clinical and neurological examinations, Mini-Mental State Examination (MMSE), and neuropsychological testing including assessment of memory function. Details of the neuropsychological assessment are shown in the Supplementary Table. Probable AD was diagnosed according to the clinical criteria of the National Institute of Neurological and Communicative Disorders and Stroke and Alzheimer's Disease and Related Disorders Association (NINCDS-ADRDA) or the criteria of the Diagnostic and Statistical Manual of Mental Disorders (DSM IV). The inclusion criterion was mild to moderate disease (MMSE score ≥20 and a Clinical Dementia Rating score of 1 or 2), and other forms of dementia (e.g. dementia with Lewy bodies) had to be excluded. All AD patients except one were under stable treatment with acetylcholinesterase inhibitors (Table 1). Additionally, neither AD patients nor control subjects were allowed to show signs of systemic autoimmune or inflammatory disease. Participants with current treatments acting on the central nervous system (including antiinflammatory treatments in prespecified time frames) were also excluded in order to avoid interference with the in vivo binding of the radioligand.

Table 1 Characteristics of the control subjects and AD patients included in the study

Subject no.		Gender	Age (years)	MMSE score	Injected dose (MBq)	Specific radioactivity (GBq/µmol)	Therapy (dose/day)
Control subjects	1	M	68	29	246	516	–
	2	M	63	30	224	79	–
	3	F	68	30	255	98	–
	4	M	73	30	273	301	–
	5	F	65	29	263	169	–
	6	M	69	28	247	250	–
	7	M	68	29	248	66	–
	Mean ± SD		68±3	29±1	251±15	211±161	
AD patients	1	M	67	28	252	195	Donepezil (10 mg)
	2	M	72	25	242	468	Galantamine (8 mg)
	3	F	71	26	251	138	Donepezil (10 mg)
	4	M	76	27	264	152	Donepezil (10 mg)
	5	F	74	23	258	139	no treatment
	6	M	67	24	254	354	Rivastigmine (6 mg)
	7	F	66	30	270	265	Galantamine (16 mg)
	8	M	65	22	257	435	Galantamine (24 mg)
	9	M	64	21	257	295	Galantamine (16 mg)
	Mean ± SD		69±4	25±3*	256±8	271±127	

*$p<0.005$ vs. control subjects, unpaired t-test.

PET experimental procedures

Precursor DAA1123 and reference standard [19F]DAA11061 were kindly provided by Bayer Schering Pharma AG. [18F]FEDAA1106 was synthesized from its precursor DAA1123 using a method described in detail elsewhere with slight modification [22]. In brief, a solution of [18F]fluoride ion in 18O-enriched water was flushed through a Sep-Pak QMA light cartridge to isolate [18F] fluoride ions. [18F]Fluoride ions were then eluted from the cartridge and the solvent was evaporated. 2-Methylbenzenesulphonate ethylbromide (15 µL) in
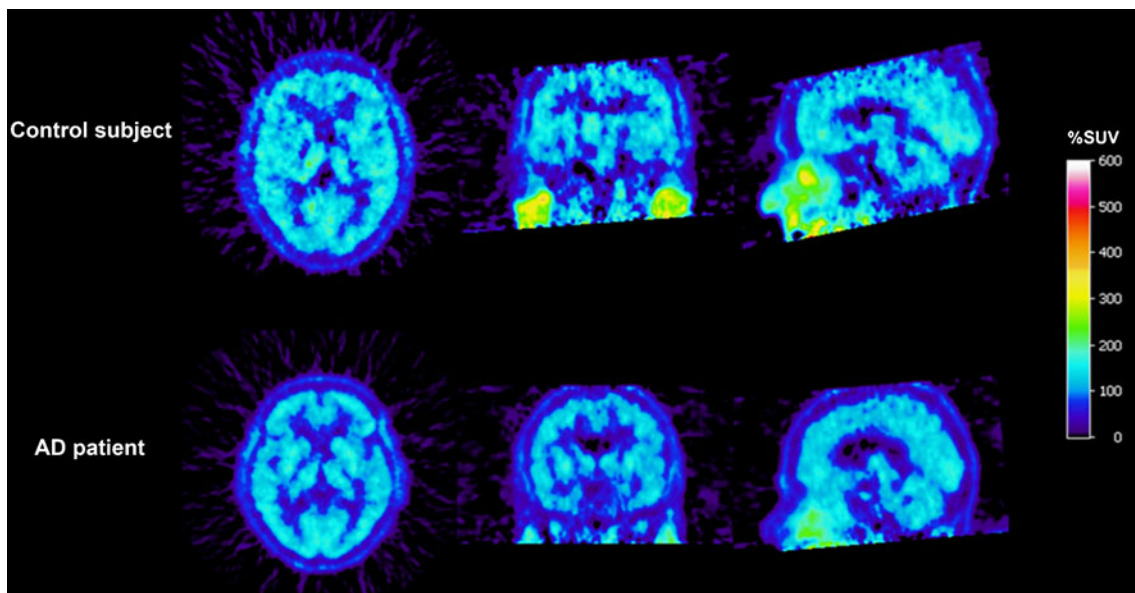

Fig. 1 Representative SUV images of [18F]FEDAA1106 from a control subject and an AD patient. The SUV images were obtained by averaging the ten frames from the second PET session from 80 to 150 min

ortho-dichlorobenzene (600 μL) was added to the [18F] fluoride ion residue and the mixture was heated at 135 °C for 10 min. The reaction mixture was cooled and the resulting [18F]fluoroethylbromide was transferred by distillation (80 °C, N_2 flow) to a second vial containing anhydrous dimethylformamide (500 μL), precursor DAA1123 (1.5–2.0 mg, 3.9–5.2 μmol) and NaOH (5 M, 15 μL) at 0 °C. The reaction mixture was heated at 110 °C for 5 min and crude [18F]FEDAA1106 was purified on a reverse-phase μBondapak C18 Semiprep HPLC column (7.8 × 300 mm, 10 μm; Waters). The fraction of the desired compound was collected and evaporated to dryness. The residue was dissolved in sterile phosphate-buffered saline (pH 7.4, 10 mL) and filtered through a sterile filter (0.22 μm; Millipore, Bedford, MA), yielding a sterile and pyrogen-free (<1.25 EU) solution of [18F]FEDAA1106.

The injected radioactivities and specific radioactivities are shown in Table 1. PET measurements were performed with an ECAT EXACT HR system (Siemens Medical Solutions, Knoxville, TN). An individual plaster helmet was made for each subject to prevent head motion during the PET measurements [23]. The acquisition protocol consisted of two PET sessions. In the first session, a transmission scan of 5 min duration was performed using three rotating 68Ge sources. Next, [18F]FEDAA1106 was injected intravenously as a bolus over 10 s and the intravenous line was immediately flushed with 10 mL NaCl. In the first session, PET measurements were acquired with a series of frames of increasing duration (6 × 20 s, 4 × 60 s, 6 × 180 s, 6 × 360 s) for a total duration of 60 min. After this first PET session, subjects were allowed to rest for 20 min outside the PET system. After this break, a second 5-min transmission scan was acquired followed by a second PET measurement of 60 min consisting of ten frames of 360 s. Images were reconstructed with filtered back projection, with a 2-mm Hanning filter, a zoom factor of 2.17, and a 128 × 128 matrix, and were corrected for attenuation and scatter [24]. Arterial blood was sampled using an automated blood sampling system (Allogg AB, Mariefred, Sweden) for the first 5 min followed thereafter by a series of manually acquired samples. Samples for metabolite analysis (HPLC) were taken at 2.5, 10, 20, 30, 40, 60, 90, 120 and 150 min after injection.

Metabolite analysis

A reverse-phase HPLC method was used to determine the percentages of radioactivity in plasma that corresponded to both unchanged [18F]FEDAA1106 and its radioactive metabolites. Plasma (0.5 mL) obtained by centrifugation of blood at 2,000 g for 2 min was mixed with acetonitrile
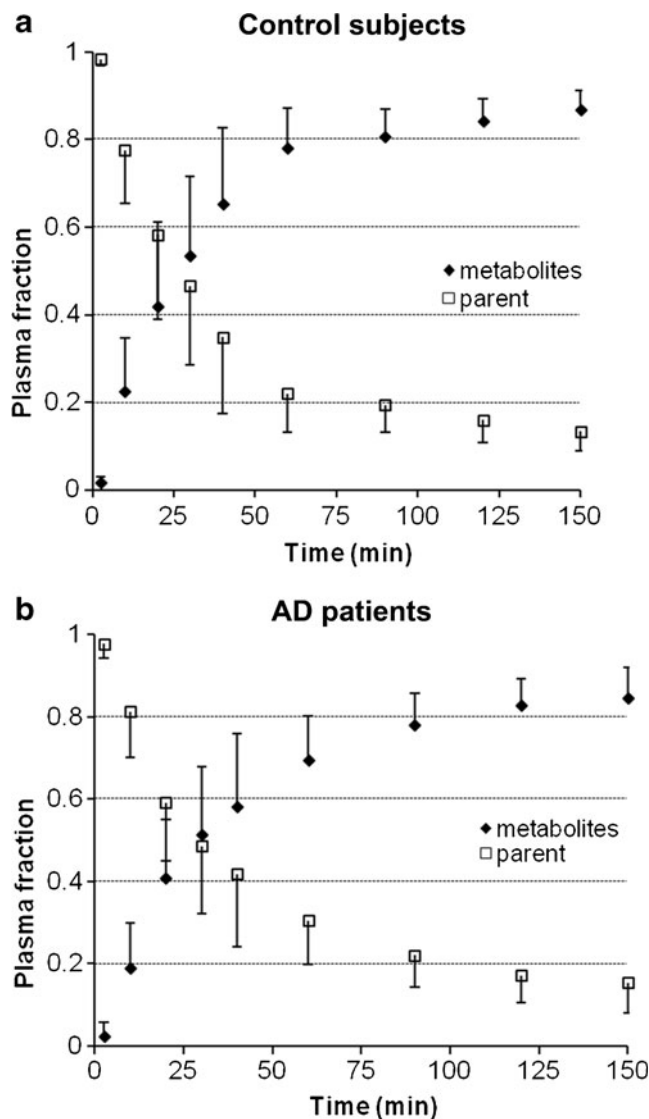

Fig. 2 Fractions of unchanged [18F]FEDAA1106 (parent) and its metabolites in control subjects (**a**) and AD patients (**b**) (*error bars* 1 SD)

(0.7 mL). After additional centrifugation of the acetonitrile/plasma mixture (1.1 mL) at 2,000 g for a further 2 min, the supernatant was measured in a NaI well-counter and then analysed using radio-HPLC.

The radio-HPLC system consisted of an interface module (D-7000; Hitachi), an L-7100 pump (Hitachi), an injector (model 7125 with a 1.0-mL loop; Rheodyne) and an absorbance detector (L-7400, 254 nm; Hitachi) in series with a radiation detector (Radiomatic 150TR; Packard) equipped with a PET Flow Cell (600 μL cell). A μ-Bondapak-C18 column (300 × 7.8 mm, 10 μm; Waters) was used for metabolite analysis. The following gradient setting was used (solvent A, acetonitrile; solvent B, 10 mM phosphoric acid): 0 min 25 % A, 75 % B; 4.5 min 80 % A, 20 % B; 8.0 min 30 % A, 70 % B; 10.0 min 25 % A, 75 % B; flow 6.0 mL/min.

Table 2 Results of kinetic analysis using NLS fitting and 2TCM (data are reported as means ± SD)

Brain region	Control subjects			AD patients		
	V_T	K_1/k_2	k_3/k_4	V_T	K_1/k_2	k_3/k_4
Frontal cortex	10.8 ± 5.5	2.2 ± 1.2	4.2 ± 1.0	13.1 ± 6.8	2.3 ± 1.3	4.7 ± 0.9
%COV	2.6 ± 1.3	5.1 ± 2.7	5.7 ± 2.8	8.8 ± 12.0	7.5 ± 4.1	13.4 ± 11.3
Orbitofrontal cortex	10.2 ± 4.8	2.2 ± 1.1	3.8 ± 0.9	12.7 ± 6.3	2.3 ± 1.2	4.5 ± 1.0
%COV	3.2 ± 1.6	6.8 ± 3.6	7.6 ± 3.9	17.1 ± 27.1	7.5 ± 2.1	21.8 ± 27.8
Anterior cingulate cortex	9.9 ± 4.7	1.9 ± 1.1	4.6 ± 1.6	8.3 ± 7.0	2.3 ± 1.1	3.3 ± 2.3
%COV	10.3 ± 6.0	17.7 ± 13.3	20.4 ± 14.2	15.8 ± 25.6	15.5 ± 5.4	22.8 ± 22.3
Temporal cortex	10.7 ± 5.3	2.1 ± 1.2	4.2 ± 0.9	11.6 ± 5.4	2.2 ± 1.1	4.5 ± 1.0
%COV	2.9 ± 1.5	5.2 ± 2.4	5.7 ± 2.4	5.7 ± 5.3	7.1 ± 3.6	9.6 ± 4.6
Insula	10.1 ± 4.8	2.1 ± 1.2	3.9 ± 0.8	11.0 ± 5.2	2.2 ± 1.1	4.1 ± 1.2
%COV	4.5 ± 2.3	7.2 ± 1.8	8.4 ± 2.4	8.6 ± 9.0	8.3 ± 2.6	12.4 ± 8.2
Posterior cingulate cortex	12.7 ± 6.9	2.9 ± 2.0	3.9 ± 1.4	32.3 ± 61.8	2.2 ± 1.5	13.7 ± 23.9
%COV	10.7 ± 9.3	11.7 ± 5.1	15.9 ± 8.7	96.6 ± 268.7	12.6 ± 5.3	104.5 ± 267.1
Parietal cortex	10.3 ± 5.1	2.0 ± 1.1	4.2 ± 0.9	13.6 ± 8.3	2.2 ± 1.2	5.3 ± 2.2
%COV	3.0 ± 1.1	6.2 ± 2.9	6.9 ± 3.0	15.9 ± 29.1	8.7 ± 3.1	21.1 ± 28.2
Occipital cortex	11.2 ± 5.8	2.2 ± 1.3	4.2 ± 1.1	12.6 ± 5.8	2.4 ± 1.3	4.6 ± 1.4
%COV	2.8 ± 1.5	7.3 ± 5.2	8.1 ± 5.5	5.7 ± 4.7	9.7 ± 5.4	11.9 ± 6.2
Hippocampus	8.8 ± 4.1	1.7 ± 1.0	4.6 ± 1.8	9.9 ± 4.8	1.9 ± 1.0	4.6 ± 1.0
%COV	4.7 ± 3.2	8.5 ± 3.7	10.0 ± 4.0	8.2 ± 6.0	10.9 ± 4.3	13.0 ± 4.4
Cerebellum	11.1 ± 5.3	2.3 ± 1.3	4.0 ± 1.0	12.5 ± 6.4	2.4 ± 1.4	4.4 ± 0.6
%COV	2.9 ± 1.7	5.4 ± 2.7	6.0 ± 2.7	6.2 ± 6.7	7.8 ± 7.1	11.1 ± 9.3
Grey matter	10.3 ± 5.0	2.1 ± 1.2	4.1 ± 0.9	11.5 ± 5.5	2.2 ± 1.2	4.4 ± 0.9
%COV	2.5 ± 1.4	5.0 ± 2.9	5.6 ± 3.0	5.9 ± 5.7	6.3 ± 2.5	9.2 ± 4.5
White matter	5.8 ± 2.0	1.0 ± 0.6	5.6 ± 2.2	6.3 ± 3.0	1.0 ± 0.6	5.6 ± 1.5
%COV	6.7 ± 2.2	7.7 ± 2.7	9.0 ± 2.5	10.3 ± 9.0	9.6 ± 4.7	13.9 ± 7.4
Caudate	9.3 ± 4.5	2.0 ± 1.1	3.9 ± 1.6	9.9 ± 4.9	2.4 ± 1.4	3.6 ± 1.5
%COV	5.2 ± 2.8	10.8 ± 4.8	12.4 ± 5.0	16.9 ± 27.9	14.0 ± 4.1	26.9 ± 29.6
Putamen	10.1 ± 4.9	2.2 ± 1.4	4.3 ± 2.0	17.9 ± 17.5	2.6 ± 1.5	5.4 ± 3.5
%COV	3.0 ± 0.9	9.0 ± 4.3	10.3 ± 4.3	83.4 ± 173.3	11.4 ± 3.5	99.4 ± 181.8
Thalamus	10.8 ± 4.8	2.2 ± 1.3	4.3 ± 1.2	17.3 ± 17.0	2.3 ± 1.4	5.9 ± 3.4
%COV	3.7 ± 1.6	7.7 ± 2.9	8.5 ± 3.1	36.5 ± 95.2	8.3 ± 3.7	42.2 ± 98.1
Midbrain	9.9 ± 4.4	1.8 ± 1.0	4.9 ± 1.7	9.8 ± 5.4	1.9 ± 0.9	4.2 ± 1.3
%COV	10.6 ± 7.1	10.5 ± 5.0	12.7 ± 5.8	9.6 ± 7.1	10.2 ± 2.5	13.7 ± 5.0
Pons	10.0 ± 4.2	1.8 ± 1.0	5.0 ± 1.8	10.4 ± 4.9	1.9 ± 1.0	4.9 ± 1.5
%COV	5.1 ± 2.2	7.7 ± 3.3	8.7 ± 3.0	8.7 ± 10.9	9.2 ± 2.8	13.3 ± 9.4

The %COV values were calculated as (standard error)/(estimate of the parameter) and represents a measure of identifiability of the parameter.

Magnetic resonance imaging

MRI was performed using a 1.5-T GE Signa system (GE Healthcare, Milwaukee, WI). MRI scans consisted of a T2-weighted sequence for ruling out pathological changes and a 3-D T1-weighted spoiled gradient recalled (SPGR) sequence for both coregistration with PET and volume-of-interest (VOI) analysis. MRI scans were evaluated for white matter changes according to the Age-Related White Matter Changes (ARWMC) scale [25], and exclusion criteria were an ARWMC score of >1 in the basal ganglia and >2 in the subcortical white matter.

Image analysis

PET images were coregistered to the T1-weighted MRI images using SPM5 (Wellcome Department of Imaging Neuroscience, London, UK). VOIs were delineated on the MRI scans using the software package Human Brain Atlas (HBA) [26]. The following regions were defined: frontal cortex, orbitofrontal cortex, temporal cortex, insula, parietal cortex, occipital cortex, anterior cingulate cortex, posterior cingulate cortex, hippocampus, caudate, putamen, thalamus, midbrain, pons, and cerebellum. A VOI for the whole grey matter (GM) was obtained from segmented MRI scans, and
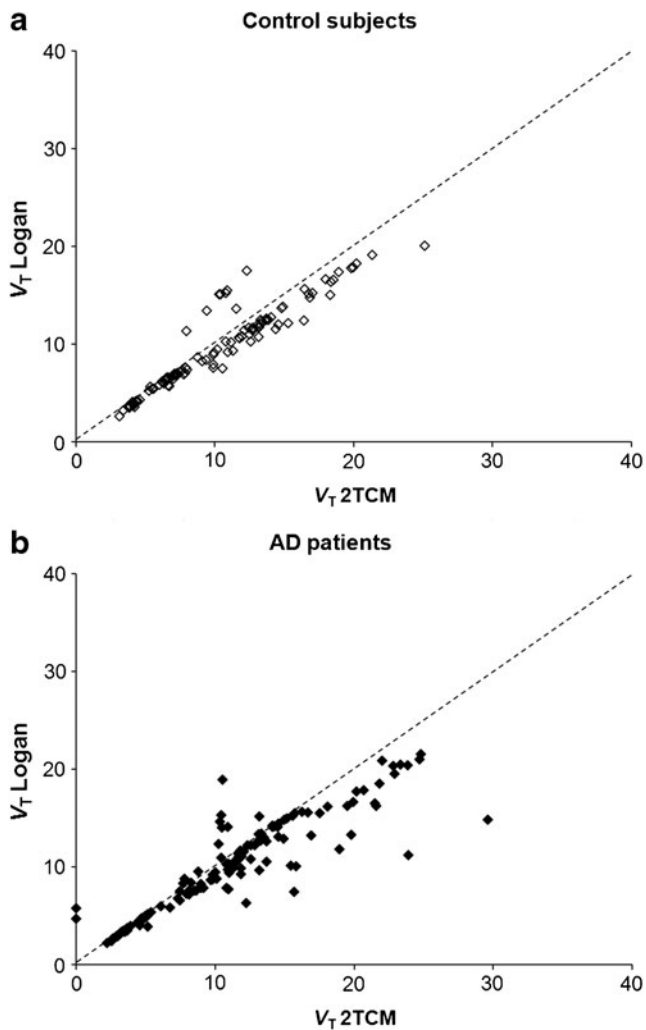
Fig. 3 Plots of V_T estimated with the 2TCM and Logan GA in control subjects (a) and AD patients (b). The *dotted line* represents the line of identity

the VOI for the white matter was obtained from the centrum semiovale.

Data analysis

Kinetic analysis was performed based on a two-tissue compartment model (2TCM), with blood volume parameter. Parameters (including fractional blood volume) for each region were fitted using NLS fitting, as implemented in software package PMOD (PMOD 3.0; PMOD Group, Zurich, Switzerland). Outcome measures were the individual rate constants K_1 (mL/g · min^{-1}) and k_2, k_3 and k_4 (min^{-1}), the total distribution volume V_T (mL/g), and the binding potential BP_{ND} obtained from the k_3/k_4 ratio estimated directly from the fits. V_T was also estimated using Logan GA. The start time (t^*) of the linear fit was estimated in each individual subject

using a preliminary fit of the time–activity curve (TAC) of the whole brain, as previously described [27].

The approach proposed by Ito et al. [28] and recently validated for [^{18}F]FEDA1106 by Ikoma et al. using Logan GA [29], was used to estimate the distribution volume of the nondisplaceable compartment (V_{ND}). In brief, the first 15 min of PET data, in which the contribution of specific binding is negligible, were used to estimate V_{ND} ($V_{ND\ 0\text{-}15\ min}$) applying Logan GA, as implemented in PMOD 3.0. The outcome measure BP_{ND} was then calculated as $V_T/V_{ND\ 0\text{-}15\ min} - 1$.

Statistical analysis

Differences between control subjects and AD patients were assessed using two-tailed unpaired *t*-tests. Differences between outcome measures obtained in the same group were assessed using two-tailed paired *t*-tests. Correlations between outcome measures were assessed using the Pearson correlation coefficient *r*. Statistical significance was set at a *p* value <0.05.

Results

Control subjects and AD patients

No statistically significant differences in age, injected radioactivity or specific radioactivity at time of injection were observed between control subjects and patients. AD patients had a significantly lower mean MMSE score than control subjects (Table 1).

PET data and HPLC analysis

A representative standardized uptake value (SUV) image of [^{18}F]FEDAA1106 in a control subject and an AD patient is shown in Fig. 1. No evidence of increased uptake in the AD patients could be seen. In the metabolite analysis no statistically significant differences in mean parent fraction or radiolabelled metabolites were observed between control subjects (Fig. 2a) and AD patients (Fig. 2b). In three subjects, the point at about 150 min was not available due to low counts in the plasma and resulting poor signal-to-noise ratios in the HPLC analysis. Therefore, the last time point was extrapolated based on the average parent fraction curve measured in control subjects and AD patients.

Kinetic analysis

Representative TACs of [^{18}F]FEDA1106 in a control subject and an AD patient and the corresponding NLS

Fig. 4 Mean values of V_T estimated with Logan GA in control subjects (*open bars*) and AD patients (*closed bars*) (*error bars* 1 SD)
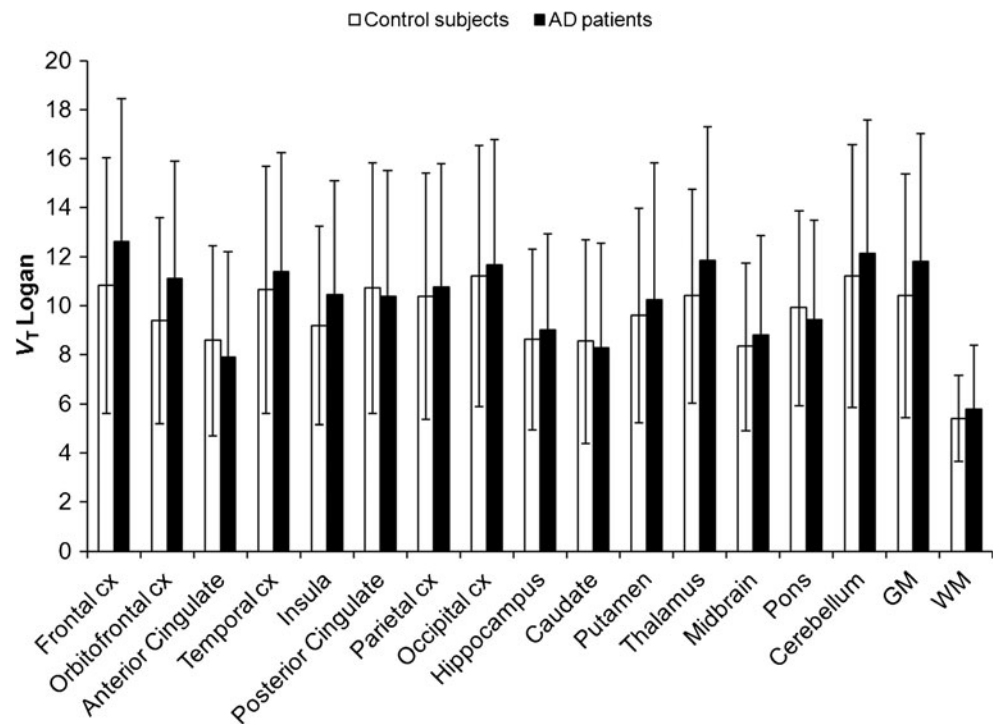
fitting are presented in Supplementary Fig. 1. No statistically significant differences in the kinetic rate constants and in K_1/k_2, V_T or BP_{ND} (k_3/k_4) were observed between groups (Table 2). Overall across all brain regions and subjects, identifiability of the main outcome measures was good as shown by a percent coefficient of variation (%COV) of the estimate of <20 %, with the exception of some brain regions (posterior cingulate cortex, putamen and thalamus) in which estimates were less accurate, probably due to low signal-to-noise ratios, leading to unrealistic estimates of the outcome measures (Table 2).

Graphical analysis

The t^* estimates were in the range 21 to 90 min (mean 41 min) in control subjects and 30 to 100 min (mean 53 min) in AD patients. The difference in mean t^* values between groups was statistically significant ($p < 0.05$). There was a statistically significant correlation ($p < 0.05$) between V_T estimates derived from the 2TCM and Logan GA in both control subjects ($r = 0.94$) and AD patients ($r = 0.90$), although there was a slight underestimation with Logan GA at the highest values of V_T (Fig. 3). This correlation was better than that V_T obtained with a fixed t^* of 48 min in all subjects (data not shown). No statistically significant difference in V_T between control subjects and AD patients was observed (Fig. 4), even when a fixed t^* of 48 min was used (data not shown).

Representative GA plots using the first 15 min of PET data are shown in Supplementary Fig. 2. A statistically

significant correlation between K_1/k_2 obtained using the 2TCM and $V_{ND\ 0-15\ min}$ obtained using Logan GA was found in control subjects ($r = 0.93$) and AD patients ($r = 0.84$) using either TACs from all brain regions (Fig. 5) or the TAC from the whole GM ($r = 0.98$ in control subjects, $r = 0.89$ in AD patients). In all cases, $V_{ND\ 0-15\ min}$ was significantly lower ($p < 0.05$) than K_1/k_2, but the difference was similar in control subjects and AD patients for both regional TACs and the TAC from the whole GM. No statistically significant difference in BP_{ND} between control subjects and AD patients was found using $V_{ND\ 0-15\ min}$ estimated using individual regional TACs (Fig. 6) or the TAC from whole GM (Supplementary Fig. 3).

Discussion

At present, imaging of TSPO is considered the most established procedure for visualizing and quantifying microglial activation as a marker of neuroinflammation. Neuroinflammatory changes have been described in several CNS disorders, including neurodegenerative disorders such as AD and Parkinson's disease. In AD, neuroinflammation appears to be an early event and microglial activation colocalizes with the deposition of amyloid in the brain. Therefore, in vivo imaging of microglial activation using TSPO radioligands appears to be a promising tool for early detection of neuroinflammation in AD patients. [^{18}F]FEDAA1106 is a radioligand for TSPO with higher binding affinity than the established radioligand [^{11}C]-(R)-PK11195, which was
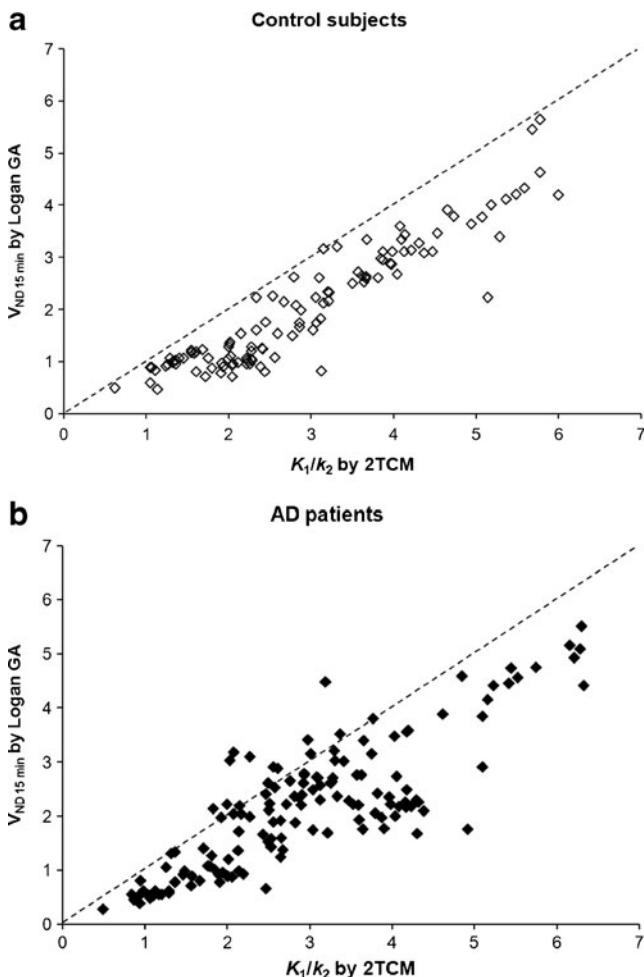
Fig. 5 Values of V_{ND} estimated with Logan GA using the first 15 min of data in relation to K_1/k_2 estimated with the 2TCM in control subjects (**a**) and AD patients (**b**). V_{ND} was estimated from the individual ROIs

developed to provide better imaging of microglial activation in vivo. This study was designed to quantify and compare the binding of [^{18}F]FEDAA1106 to TSPO in the brain of control subjects and AD patients.

The main finding of this study was that no statistically significant increase in TSPO binding in AD patients could be found using [^{18}F]FEDAA1106, although overall trends towards higher V_T and BP_{ND} values in AD patients were observed. Because of these findings, some issues related to the kinetic properties of the radioligand and to the biological or pathophysiological properties of TSPO should be considered.

Kinetic properties and quantification of [^{18}F]FEDAA1106

Due the lack of a suitable reference region in the brain devoid of specific binding, [^{18}F]FEDAA1106 requires invasive quantification with the measurement of the arterial input function. [^{18}F]FEDAA1106 has a very slow washout from the brain and requires at least 120 to 150 min of image

acquisition [21]. Therefore, the accuracy of the estimation of outcome measures such as V_T or k_3/k_4 can be influenced by the accuracy of the blood and plasma measurements and metabolite analysis, particularly for the latest time points, at which the counting statistics and the signal-to-noise ratio might be low.

To overcome the limitations related to the measurement of the arterial input function, a reference tissue method could be a suitable alternative. In the case of [^{11}C]-(R)-PK11195 previous studies have shown that the cerebellum is a suitable reference region and that supervised cluster analysis is a valid approach to extract a reference tissue curve for noninvasive quantification of BP_{ND} [30–32]. This latter approach requires the definition of specific kinetic clusters obtained from data showing a clear increase in specific binding signal, such as those obtained in patients with brain trauma. These data are available for [^{11}C]-(R)-PK11195, but not for [^{18}F]FEDAA1106. Therefore, the utility of supervised cluster analysis at present cannot be evaluated for [^{18}F]FEDAA1106.

In theory, estimation of the outcome measure V_T should be independent of K_1. In the present study, however, estimation of V_T was dependent on K_1 in both control subjects and AD patients (Supplementary Fig. 4). The reason for this dependency of V_T on K_1 is not completely understood. One explanation could be a slow plasma equilibration of the radioligand. When plotting the plasma-to-blood radioactivity ratio as function of time, in all subjects a consistent increase from approximately 10 to 15 min after injection was observed (Supplementary Fig. 5), which might suggest slow equilibration of [^{18}F]FEDAA1106 between the blood cells (probably the white blood cells) and plasma. This slow equilibration might have contributed to a lower identifiability of k_3 (%COV 15.5 ± 8.5 % in controls and 20.3 ± 12.7 % in AD patients) compared with K_1 (%COV 3.0 ± 1.8 % in controls and 3.1 ± 1.3 % in AD patients) in the 2TCM, resulting in an estimate of V_T more dependent on K_1 (i.e. cerebral blood flow and delivery). Finally, possible radiolabelled metabolite(s) entering the brain might have produced a bias in the estimation of V_T. Overall, the kinetic behaviour makes it difficult to use [^{18}F]FEDAA1106 in in vivo imaging and quantification of TSPO and probably contributed to the large variability in V_T (approximate %COV 40–50 %) observed in both controls and AD patients.

Graphical analysis vs. NLS fitting

The outcome measure V_T used for the comparison between AD patients and control subjects was obtained with Logan GA. GA is often associated with underestimation of V_T as compared with NLS fitting, due to intrinsic noise in the PET data [33]. However, GA was chosen because NLS fitting provided erroneous estimates of V_T in some small

Fig. 6 Mean values of BP_{ND} calculated as $V_T/V_{ND\ 0\text{-}15\ min} - 1$ with Logan GA in control subjects (*open bars*) and AD patients (*closed bars*). $V_{ND\ 0\text{-}15\ min}$ was estimated from the individual ROIs (*error bars* 1 SD)
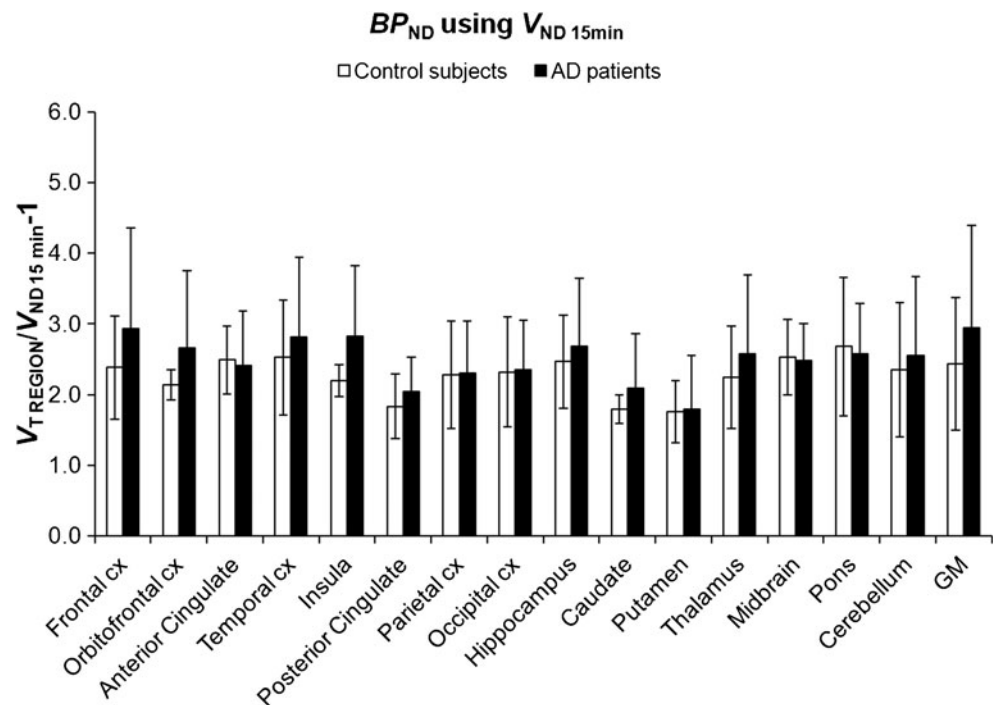
brain regions due to noise in the data. The estimation of t^* using $[^{18}F]$FEDAA1106 is difficult due to its slow kinetics [21]. For this reason, V_T was obtained using t^* values estimated for each subject, since this approach provided better agreement with NLS fitting than V_T obtained using fixed t^* values.

In this study we also used a GA method based on the analysis of the first 15 min of PET data to estimate V_{ND}. The use of this method has already been described for $[^{18}F]$FEDAA1106. It is based on the assumption that at early time points the contribution of the specific binding is negligible, an therefore the slope of the linear plot provides an estimate of V_{ND} [29]. This method provides estimates of BP_{ND} that correlate with the outcome measure obtained with the 2TCM, despite some underestimation [29]. We found that V_{ND} was underestimated relative to the ratio K_1/k_2 obtained from NLS fitting. This underestimation could have been related to the slow kinetics of $[^{18}F]$FEDAA1106 and to the difficulty in separating the fast from the slow equilibrating compartments.

Biological and pathophysiological aspects related to TSPO

The large variability in V_T amongst subjects could also have been due to biological heterogeneity in both controls and AD patients. It is known that a polymorphism of the TSPO gene is responsible for subjects having very different binding affinities for the high-affinity TSPO radioligand (N-{2-(methyloxy)phenyl]methyl}-N-[4-(phenyloxy)-3-pyridinyl]acetamide (PBR28) [34]. In the case of PBR28, three different binding affinity profiles, i.e. low-affinity, mixed-affinity and high-affinity, have been described based on in vitro binding competition experiments with $[^3H]$PK11195 and PBR28 [35]. Other TSPO radioligands, such as N,N-diethyl-2-[2-(4-methoxyphenyl)-5,7-dimethyl-pyrazolo[1,5-a]pyrimidin-3-yl]-acetamide (DPA-713) and DAA1106 also show different binding affinity profiles in vitro, although the difference between high-affinity and low-affinity binders is much smaller than for PBR28 [35]. In vitro binding data for FEDAA1106 are not available, neither were blood samples collected in this study to examine the presence of different binding affinity profiles, as this information was not available at the time the study was designed and conducted. However, the presence of subjects with a lower affinity binding site could have contributed to the large variability in V_T observed in this study.

The other outcome measures examined in this study were k_3/k_4 estimated using NLS and the 2TCM and BP_{ND} calculated from distribution volumes using Logan GA. Both outcome measures (and in particular k_3/k_4) displayed lower variability compared with V_T. However, neither outcome measure seemed to improve the differentiation between controls and AD patients. A recent study in controls and AD patients using the radioligand $[^{11}C]$DAA1106 showed significantly higher k_3/k_4 in the prefrontal cortex, parietal cortex, lateral temporal cortex, anterior cingulate and striatum of AD patients [19]. The reason for this discrepancy in relation to the present results is not clear but could be because of differences in the AD patients recruited, differences in radioligands (higher k_3/k_4 in case of $[^{11}C]$DAA1106), and differences

in the proportion of subjects with low-affinity binding sites, considering the reported difference in the prevalence of the TSPO polymorphism between Caucasian and Asian populations [34].

It is possible that the degree of microglial activation in AD cannot be detected reliably in vivo using [^{18}F]FEDAA1106. A recent in vitro autoradiography study with [^{125}I]desfluoro-DAA1106 has shown increased specific binding of the radioligand in the temporal and parietal cortices of AD patients compared with control subjects [36]. The specific and nonspecific binding of [^{18}F]FEDAA1106 cannot be separated in vivo as can be done in vitro in tissue sections, and therefore it is possible that the relatively high nonspecific binding of [^{18}F]FEDAA1106 did not allow an increased specific signal to be detected. An in vivo study in subjects with mild cognitive impairment (MCI) and patients with AD using the radioligand [^{11}C]deprenyl-D$_2$, measuring MAO-B activity as a marker of astrocyte activation (and neuroinflammation), showed increased binding in MCI subjects, but not in AD patients, compared with controls [37]. Therefore, it is also possible that neuroinflammation is a rather early event in the natural history of AD, which would be difficult to measure in vivo at the stage of clinically developed AD using currently available imaging methods.

Finally, almost all AD patients were on treatment with cholinesterase inhibitors. Although it would have been preferable to include only drug-naive patients, it is difficult to achieve this in the clinical setting. We believe that the interaction between treatment with cholinesterase inhibitors and the TSPO binding would be negligible. Since no patient was allowed to be receiving antiinflammatory treatment, we believe that pharmacological treatment was not a major confounder in this study.

Conclusion

Binding of [^{18}F]FEDAA1106 to TSPO was not significantly higher in AD patients than in controls. Therefore, [^{18}F]FEDAA1106 does not seem to be a promising tool for the in vivo detection of microglial activation in AD.

References

1. Rupprecht R, Papadopoulos V, Rammes G, Baghai TC, Fan J, Akula N, et al. Translocator protein (18 kDa) (TSPO) as a therapeutic target for neurological and psychiatric disorders. Nat Rev Drug Discov. 2010;9:971–88.
2. Scarf AM, Kassiou M. The translocator protein. J Nucl Med. 2011;52:677–80.
3. Bird JL, Izquierdo-Garcia D, Davies JR, Rudd JH, Probst KC, Figg N, et al. Evaluation of translocator protein quantification as a tool for characterising macrophage burden in human carotid atherosclerosis. Atherosclerosis. 2010;210:388–91.
4. Cosenza-Nashat M, Zhao ML, Suh HS, Morgan J, Natividad R, Morgello S, et al. Expression of the translocator protein of 18 kDa by microglia, macrophages and astrocytes based on immunohistochemical localization in abnormal human brain. Neuropathol Appl Neurobiol. 2009;35:306–28.
5. Kuhlmann AC, Guilarte TR. Cellular and subcellular localization of peripheral benzodiazepine receptors after trimethyltin neurotoxicity. J Neurochem. 2000;74:1694–704.
6. Venneti S, Lopresti BJ, Wiley CA. Molecular imaging of microglia/macrophages in the brain. Glia. 2013;61:10–23.
7. Pappata S, Levasseur M, Gunn RN, Myers R, Crouzel C, Syrota A, et al. Thalamic microglial activation in ischemic stroke detected in vivo by PET and [11C]PK1195. Neurology. 2000;55:1052–4.
8. Ramlackhansingh AF, Brooks DJ, Greenwood RJ, Bose SK, Turkheimer FE, Kinnunen KM, et al. Inflammation after trauma: microglial activation and traumatic brain injury. Ann Neurol. 2011;70:374–83.
9. Banati RB, Newcombe J, Gunn RN, Cagnin A, Turkheimer F, Heppner F, et al. The peripheral benzodiazepine binding site in the brain in multiple sclerosis: quantitative in vivo imaging of microglia as a measure of disease activity. Brain. 2000;123 (Pt 11):2321–37.
10. Cagnin A, Brooks DJ, Kennedy AM, Gunn RN, Myers R, Turkheimer FE, et al. In-vivo measurement of activated microglia in dementia. Lancet. 2001;358:461–7.
11. Gerhard A, Pavese N, Hotton G, Turkheimer F, Es M, Hammers A, et al. In vivo imaging of microglial activation with [11C](R)-PK11195 PET in idiopathic Parkinson's disease. Neurobiol Dis. 2006;21:404–12.
12. Halliday G, Robinson SR, Shepherd C, Kril J. Alzheimer's disease and inflammation: a review of cellular and therapeutic mechanisms. Clin Exp Pharmacol Physiol. 2000;27:1–8.
13. Akiyama H, Arai T, Kondo H, Tanno E, Haga C, Ikeda K. Cell mediators of inflammation in the Alzheimer disease brain. Alzheimer Dis Assoc Disord. 2000;14 Suppl 1:S47–53.
14. Chaki S, Funakoshi T, Yoshikawa R, Okuyama S, Okubo T, Nakazato A, et al. Binding characteristics of [3H]DAA1106, a novel and selective ligand for peripheral benzodiazepine receptors. Eur J Pharmacol. 1999;371:197–204.
15. Dolle F, Luus C, Reynolds A, Kassiou M. Radiolabelled molecules for imaging the translocator protein (18 kDa) using positron emission tomography. Curr Med Chem. 2009;16:2899–923.
16. Maeda J, Suhara T, Zhang MR, Okauchi T, Yasuno F, Ikoma Y, et al. Novel peripheral benzodiazepine receptor ligand [11C]DAA1106 for PET: an imaging tool for glial cells in the brain. Synapse. 2004;52:283–91.
17. Zhang MR, Maeda J, Furutsuka K, Yoshida Y, Ogawa M, Suhara T, et al. [18F]FMDAA1106 and [18F]FEDAA1106: two positron-emitter labeled ligands for peripheral benzodiazepine receptor (PBR). Bioorg Med Chem Lett. 2003;13:201–4.
18. Ikoma Y, Yasuno F, Ito H, Suhara T, Ota M, Toyama H, et al. Quantitative analysis for estimating binding potential of the peripheral benzodiazepine receptor with [(11)C]DAA1106. J Cereb Blood Flow Metab. 2007;27:173–84.
19. Yasuno F, Ota M, Kosaka J, Ito H, Higuchi M, Doronbekov TK, et al. Increased binding of peripheral benzodiazepine receptor in Alzheimer's disease measured by positron emission tomography with [11C]DAA1106. Biol Psychiatry. 2008;64:835–41.
20. Zhang MR, Maeda J, Ogawa M, Noguchi J, Ito T, Yoshida Y, et al. Development of a new radioligand, N-(5-fluoro-2-phenoxyphenyl)-N-(2-[18F]fluoroethyl-5-methoxybenzyl)acetamide, for pet imaging of peripheral benzodiazepine receptor in primate brain. J Med Chem. 2004;47:2228–35.

21. Fujimura Y, Ikoma Y, Yasuno F, Suhara T, Ota M, Matsumoto R, et al. Quantitative analyses of 18F-FEDAA1106 binding to peripheral benzodiazepine receptors in living human brain. J Nucl Med. 2006;47:43–50.
22. Takano A, Gulyas B, Varrone A, Karlsson P, Sjoholm N, Larsson S, et al. Biodistribution and radiation dosimetry of the 18 kDa translocator protein (TSPO) radioligand [18F]FEDAA1106: a human whole-body PET study. Eur J Nucl Med Mol Imaging. 2011;38:2058–65.
23. Bergstrom M, Boethius J, Eriksson L, Greitz T, Ribbe T, Widen L. Head fixation device for reproducible position alignment in transmission CT and positron emission tomography. J Comput Assist Tomogr. 1981;5:136–41.
24. Wienhard K, Dahlbom M, Eriksson L, Michel C, Bruckbauer T, Pietrzyk U, et al. The ECAT EXACT HR: performance of a new high resolution positron scanner. J Comput Assist Tomogr. 1994;18:110–8.
25. Wahlund LO, Barkhof F, Fazekas F, Bronge L, Augustin M, Sjogren M, et al. A new rating scale for age-related white matter changes applicable to MRI and CT. Stroke. 2001;32:1318–22.
26. Roland PE, Geyer S, Amunts K, Schormann T, Schleicher A, Malikovic A, et al. Cytoarchitectural maps of the human brain in standard anatomical space. Hum Brain Mapp. 1997;5:222–7.
27. Varrone A, Toth M, Steiger C, Takano A, Guilloteau D, Ichise M, et al. Kinetic analysis and quantification of the dopamine transporter in the nonhuman primate brain with 11C-PE2I and 18F-FE-PE2I. J Nucl Med. 2011;52:132–9.
28. Ito H, Yokoi T, Ikoma Y, Shidahara M, Seki C, Naganawa M, et al. A new graphic plot analysis for determination of neuroreceptor binding in positron emission tomography studies. Neuroimage. 2010;49:578–86.
29. Ikoma Y, Takano A, Varrone A, Halldin C. Graphic plot analysis for estimating binding potential of translocator protein (TSPO) in positron emission tomography studies with [(18)F]FEDAA1106. Neuroimage. 2012;69C:78–86.
30. Kropholler MA, Boellaard R, van Berckel BN, Schuitemaker A, Kloet RW, Lubberink MJ, et al. Evaluation of reference regions for (R)-[(11)C]PK11195 studies in Alzheimer's disease and mild cognitive impairment. J Cereb Blood Flow Metab. 2007;27:1965–74.
31. Turkheimer FE, Edison P, Pavese N, Roncaroli F, Anderson AN, Hammers A, et al. Reference and target region modeling of [11C]-(R)-PK11195 brain studies. J Nucl Med. 2007;48:158–67.
32. Yaqub M, van Berckel BN, Schuitemaker A, Hinz R, Turkheimer FE, Tomasi G, et al. Optimization of supervised cluster analysis for extracting reference tissue input curves in (R)-[(11)C]PK11195 brain PET studies. J Cereb Blood Flow Metab. 2012;32:1600–8.
33. Slifstein M, Laruelle M. Effects of statistical noise on graphic analysis of PET neuroreceptor studies. J Nucl Med. 2000;41:2083–8.
34. Owen DR, Yeo AJ, Gunn RN, Song K, Wadsworth G, Lewis A, et al. An 18-kDa translocator protein (TSPO) polymorphism explains differences in binding affinity of the PET radioligand PBR28. J Cereb Blood Flow Metab. 2012;32:1–5.
35. Owen DR, Gunn RN, Rabiner EA, Bennacef I, Fujita M, Kreisl WC, et al. Mixed-affinity binding in humans with 18-kDa translocator protein ligands. J Nucl Med. 2011;52:24–32.
36. Gulyas B, Makkai B, Kasa P, Gulya K, Bakota L, Varszegi S, et al. A comparative autoradiography study in post mortem whole hemisphere human brain slices taken from Alzheimer patients and age-matched controls using two radiolabelled DAA1106 analogues with high affinity to the peripheral benzodiazepine receptor (PBR) system. Neurochem Int. 2009;54:28–36.
37. Carter SF, Scholl M, Almkvist O, Wall A, Engler H, Langstrom B, et al. Evidence for astrocytosis in prodromal Alzheimer disease provided by 11C-deuterium-L-deprenyl: a multitracer PET paradigm combining 11C-Pittsburgh compound B and 18F-FDG. J Nucl Med. 2012;53:37–46.